Iterative Time-Variant Channel Estimation for 802.11p Using Generalized Discrete Prolate Spheroidal Sequences

Thomas Zemen, *Senior Member, IEEE*, Laura Bernadó, *Student Member, IEEE*, Nicolai Czink, *Member, IEEE*, and Andreas F. Molisch, *Fellow, IEEE*

***Abstract*—This paper deals with channel estimation for orthogonal frequency-division multiplexing (OFDM) in time-variant wireless propagation channels. We particularly consider the challenges of the IEEE 802.11p standard, which is the worldwide dominant system for vehicular communications. For historic reasons, 802.11p uses a pilot pattern that is identical to the pattern used in 802.11a, which was initially designed for the estimation of indoor channels with little or no time variations. Therefore, this pilot pattern violates the sampling theorem for channels with both large delay spread and large Doppler spread, as often occurs in vehicular communications. To remedy this problem, we design a robust iterative channel estimator based on a 2-D subspace spanned by generalized discrete prolate spheroidal sequences. Due to the tight subspace design, the iterative receiver is able to converge to the same bit error rate (BER) as a receiver with perfect channel knowledge. Furthermore, we propose a backward compatible modification of the 802.11p pilot pattern such that the number of iterations sufficient for convergence can be reduced by a factor of 2–3, strongly reducing implementation complexity.**

***Index Terms*—Generalized discrete prolate spheroidal sequences, IEEE 802.11p, intelligent transportation system, time-variant channel estimation, wireless vehicular communications.**

I. Introduction

WIRELESS communications for vehicle-to-vehicle or vehicle-to-infrastructure scenarios has many important applications, including collision avoidance, reduction of traffic congestion, wrong-way driving warning, as well as enabling e-mobility [1], and thus has drawn great attention over the past few years. An international standard, i.e., wireless access in vehicular environments [2], has been developed. Its physical layer is based on the 802.11p standard [3]. It is the main candidate for implementation by major car manufacturers and is supported by various programs, in particular in the European Union and Japan.

A main challenge of vehicular communications is the rapidly changing radio propagation conditions. Many measurement campaigns have demonstrated high Doppler and delay spreads and even nonstationarities of the channel statistics (see [1] and [4] for an overview and further references). Consequently, robust channel estimation is particularly important, but also particularly difficult, in such an environment.

The challenges are exacerbated by the design of training signals in the 802.11p standard. To exploit existing chip designs and economies of scale, this standard is virtually identical to the well-known IEEE 802.11a/g (WiFi) standard. However, while the training signal design works well for environments where WiFi is normally operating in (i.e., indoor environments with little or no mobility), it does not work in conjunction with standard channel estimation techniques in many vehicular propagation channels, namely, those that have large delay and Doppler spreads.

To combat difficulties in time-variant wireless channels, we can exploit the fact that the time-variant frequency-selective impulse responses of the channels are restricted to low-dimensional subspaces. Further improvements can be achieved by iterations between channel estimation and symbol decisions.

Related Literature: A number of publications investigate the performance of 802.11p [1], [5]–[7] in a realistic vehicular channel with both large delay and Doppler spreads, demonstrating the need for improved algorithms. Parallel to the present work, [8] shows an improved orthogonal frequency-division multiplexing (OFDM) symbol-wise decision-directed channel estimation method that does not need a standard modification but is limited to frame error rates (FERs) in the order of 10^{-1}. In [9], OFDM symbol-wise decision together with smoothing in the frequency domain and antenna diversity is investigated. In [10], a modified physical layer in the form of time-domain differential modulation is proposed to remove the need for time-variant channel estimation. The insertion of additional pilot symbols is advocated in a nonbackward compatible fashion in [11] and [12].

However, it turns out that it is difficult to reach an FER below 10^{-1} in vehicular channels with the 802.11p pilot pattern. Hence, low-complexity robust frame-based channel estimation methods must be investigated such that the correlation of the

Manuscript received August 26, 2011; revised December 9, 2011; accepted January 10, 2012. Date of publication January 23, 2012; date of current version March 21, 2012. This work was supported in part by the industry partners, the Austrian Government, and the City of Vienna within the competence center program COMET. The work of T. Zemen, L. Bernadó, and N. Czink was also supported in part by the FTW project NOWIRE funded by the Vienna Science and Technology Fund and in part by NFN SISE S106 funded by the Austrian Science Fund. The review of this paper was coordinated by Dr. H. Lin.

T. Zemen, L. Bernadó, and N. Czink are with the FTW Telecommunications Research Center Vienna, Vienna, Austria (e-mail: thomas.zemen@ftw.at; bernado@ftw.at; czink@ftw.at).

A. F. Molisch is with the University of Southern California, Los Angeles, CA 90037 USA (e-mail: molisch@usc.edu).

Color versions of one or more of the figures in this paper are available online at http://ieeexplore.ieee.org.

Digital Object Identifier 10.1109/TVT.2012.2185526

fading process can jointly be exploited in time and frequency. At the same time, the algorithm must also be robust toward the nonstationary nature of the vehicular communication channel.

A number of existing papers deal with channel estimation in time-variant channels based on subspaces. In [13], a low-dimensional subspace spanned by discrete prolate spheroidal (DPS) sequences [14] is used. The subspace is designed according to the given maximum normalized Doppler shift $\nu_{\mathrm{Dmax}} = \upsilon_{\max} f_C T_S / c_0$, which is determined by the maximum velocity $\upsilon_{\max}$, the carrier frequency f_C, the speed of light c_0, and the symbol duration T_S. The square channel estimation bias obtained with the Slepian basis expansion is more than a magnitude smaller compared with the Fourier basis expansion (i.e., a truncated discrete Fourier transform) [15].

While [13] estimates the Slepian basis expansion coefficients individually for every subcarrier in an OFDM system, further improvements can be obtained by exploiting the correlation between the individual subcarriers in the frequency domain. For this purpose, a truncated Fourier transform was used in [16]. However, this approach is optimal only for sample-spaced path delays. For more realistic real-valued path delays, Edfors *et al.* [17] exploited the correlation in the frequency domain by using the singular value decomposition (SVD) of the channel covariance matrix, which is assumed to be known. In [18], the SVD was calculated in an adaptive manner using an estimate of the covariance matrix. In [19] and [20], a 2-D Wiener filter is employed for time and frequency selective channel estimations.

Iterative channel estimation, i.e., alternate payload data estimation and channel estimation, has been discussed in a number of papers (see, e.g., [21]–[26]). The 2-D Wiener filter is employed for iterative channel estimation in [27]. In [27], a reduced-complexity SVD-based low-rank approximation [28], [29] is shown as well.

In [30], two successive Slepian subspace projections are used for time-variant frequency-selective channel estimation. This allows exploiting the correlation in the time and frequency domain without the need to estimate the channel covariance function and to perform an SVD. A 2-D projection on a fixed Slepian subspace is further explored in [31]. However, the subspace in the frequency domain is chosen twice as large as necessary (cf. [31, paragraph after eq. (2)]).

Contributions of This Paper:

1) We further tighten the 2-D subspace of [31] by using generalized DPS sequences [32] that allow for a generalized nonsymmetric (and even discontiguous) band limit in the time and frequency domains. With a tight subspace, we can further reduce the channel estimation mean square error (MSE).
2) We validate the time-variant channel estimator using a geometry-based stochastic channel model (GSCM) in an 802.11p-compliant link-level simulation [33]. The channel model is obtained from vehicular channel measurements [34].
3) We show that, with a tight subspace design, near-optimal channel estimation can still be obtained iteratively in an 802.11p compliant system, despite the aforementioned deficiencies of the training signal design in this standard.
4) Finally, we propose a transparent backward-compatible extension to the 802.11p standard allowing for reduced-complexity channel estimation. This is achieved by adding an additional OFDM pilot symbol to the end of the otherwise standard compliant frame and by utilizing one of the reserved header bits.

Notation: We denote a scalar by a, a column vector by $\boldsymbol{a}$, and its ith element with $a[i]$. Similarly, we denote a matrix by $\boldsymbol{A}$ and its (i,ℓ)th element by $[\boldsymbol{A}]_{i,\ell}$. The transpose of $\boldsymbol{A}$ is given by $\boldsymbol{A}^{\mathrm{T}}$ and its conjugate transpose by $\boldsymbol{A}^{\mathrm{H}}$. A diagonal matrix with elements $a[i]$ is written as $\mathrm{diag}(\boldsymbol{a})$ and the $Q \times Q$ identity matrix as $\boldsymbol{I}_Q$. The absolute value of a is denoted by $|a|$ and its complex conjugate by a^*. The largest (smallest) integer that is lower (greater) than or equal to $a \in \mathbb{R}$ is denoted by $\lfloor a \rfloor$ ($\lceil a \rceil$). We denote the set of all integers by $\mathbb{Z}$, the set of real numbers by $\mathbb{R}$, and the set of complex numbers by $\mathbb{C}$.

Organization of This Paper: The OFDM signal model is presented in Section II. In Section III, we introduce the GSCM used to simulate the time-variant impulse response of a vehicular communication channel. For channel estimation at the receiver side, a subspace channel model based on generalized DPS sequences is presented in Section IV and the corresponding iterative estimator in Section V. In Section VI, the 802.11p pilot pattern and our proposed enhancement are discussed. The numeric simulation results are shown in Section VII together with a discussion of the iterative receiver complexity. We draw conclusions in Section VIII.

II. Signal Model

We consider the equalization and detection problem for an OFDM link [35], [36]. The OFDM system utilizes N subcarriers and a cyclic prefix with length G. The transmission is frame oriented with frame length M and utilizes a bandwidth B and the sampling rate at the receiver side $1/T_C = B$. The OFDM symbol duration is given by $T_S = (N+G)T_C$.

Each frame contains $S = |\mathcal{S}|$ coded data symbols $b[m,q]$ $\forall\ [m,q] \in \mathcal{S}$, where $m \in \mathcal{I}_M = \{0,\ldots,M-1\}$ denotes the discrete time at rate $1/T_S$, $q \in \mathcal{I}_N$ denotes the subcarrier index with frequency spacing $1/(T_C N)$, and $\mathcal{S}$ denotes the 2-D data symbol position index set in the time–frequency plane, respectively. For $[m,q] \notin \mathcal{S}$, we define $b[m,q] = 0$.

A binary information sequence $\chi[m'']$ of length $2SR_C$ is convolutionally encoded with code rate R_C, resulting in a sequence of code bits $c[m']$ (see Fig. 1). After interleaving and quadrature phase-shift keying (QPSK) modulation with Gray labeling, the data symbols are mapped on the OFDM time–frequency grid as

$$b[\mathcal{S}_s] = \frac{1}{\sqrt{2}}\left(c[2s] + jc[2s+1]\right) \qquad \forall s \in \mathcal{I}_S \qquad (1)$$

where $\mathcal{S}_s$ denotes the sth element $[m_s, q_s]$ of the set $\mathcal{S}$ in the OFDM time–frequency grid.

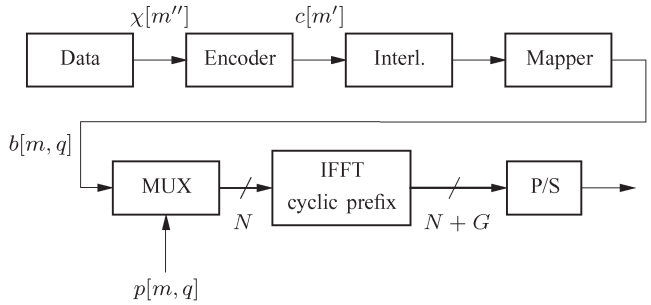

Fig. 1. Model of the OFDM transmitter.

In each frame, $J = |\mathcal{P}|$ pilot symbols $p[m,q]\ \forall\ [m,q] \in \mathcal{P}$ are transmitted, where $\mathcal{P}$ denotes the pilot symbol position index. For $[m,q] \notin \mathcal{P}$, we define $p[m,q] = 0$. The two sets $\mathcal{P}$ and $\mathcal{S}$ are nonoverlapping. The pilot symbols $p[m,q]$ are added, giving

$$d[m,q] = b[m,q] + p[m,q]. \tag{2}$$

Subsequently, an N-point inverse discrete Fourier transform is carried out, and a cyclic prefix of length G is inserted. An OFDM symbol, including the cyclic prefix, has length $N+G$ samples.

The time-variant frequency response

$$g(t,f) = g_{\mathrm{Tx}}(f) g_{\mathrm{Ph}}(t,f)_{\mathrm{Rx}}(f) \tag{3}$$

contains the effects of the physical (nonband-limited) channel $g_{\mathrm{Ph}}(t,f)$ as well as the band-limiting filter at the transmitter side $g_{\mathrm{Tx}}(f)$ and the receiver side $g_{\mathrm{Rx}}(f)$, respectively. The sampled time-variant frequency response, which is used for channel simulation, is defined as

$$g'[n,q] := g\left(nT_C, \varphi(q)/(NT_C)\right). \tag{4}$$

The function $\varphi(q) = ((q + N/2 \bmod N) - N/2)$ maps the subcarrier index $q \in \{0,\ldots,N-1\}$ into the discrete frequency index $\varphi = \{0,\ldots,N/2-1,-N/2,\ldots,-1\}$.

Generally, in an OFDM system, intercarrier interference is caused by a time-variant channel impulse response. However, if the normalized Doppler bandwidth ν_{D} stays below a fraction $\epsilon = 5 \cdot 10^{-1}$ of the normalized subcarrier bandwidth

$$\frac{\nu_D N}{N+G} < \epsilon \tag{5}$$

the intercarrier interference is small enough to be neglected for processing at the receiver side [37]–[39].

This condition is well fulfilled for IEEE 802.11p systems up to a velocity of about 1440 km/h to 400 m/s. Hence, we are able to define the sampled time-variant channel as $g[m,q] := g(m(N+G)T_C, \varphi(q)/(NT_C)) = g'[m(N+G),q]$, temporally sampled at rate $(N+G)/T_C$ for processing at the receive side. We can do this since the intercarrier interference is expected to have only a minor impact on the receiver performance. For the channel simulation, we use $g'[n,q]$ sampled at rate $1/T_C$; hence, all intercarrier interference effects are fully present in the received signal.

The received signal after cyclic prefix removal and discrete Fourier transform is

$$y[m,q] = g[m,q]d[m,q] + z[m,q] \tag{6}$$

where circularly symmetric complex white Gaussian noise with zero mean and covariance σ_z^2 is denoted by $z[m,q]$. The output of a minimum MSE (MMSE) equalizer

$$\hat{d}[m,q] = \frac{y[m,q]\hat{g}[m,q]^*}{\sigma_z^2 + |\hat{g}[m,q]|^2} \tag{7}$$

is used as input to a Bahl–Cocke–Jelinek–Raviv (BCJR) decoder [40] after demapping and deinterleaving. In (7), we denote by $\hat{g}[m,q]$ the channel estimate at time index m and subcarrier index q.

III. Geometry-Based Stochastic Model for Wireless Wave Propagation

The time-variant frequency response

$$g(t,f) = g_{\mathrm{Tx}}(f) \underbrace{\left(\sum_{\ell=0}^{P-1} \eta_\ell(t) \mathrm{e}^{-\mathrm{j}2\pi\tau_\ell(t)f}\right)}_{g_{\mathrm{Ph}}(t,f)} g_{\mathrm{Rx}}(f) \tag{8}$$

can be described as the superposition of P individual paths, given P is sufficiently large. Each path is characterized by the complex time-variant weighting coefficient $\eta_\ell(t)$ and its real-valued time-variant delay $\tau_\ell(t)$.

We can approximate the nonstationary fading process as wide-sense stationary for the duration of a single OFDM frame $m \in \mathcal{I}_M$ and $q \in \mathcal{I}_N$ [41], [42]. Hence, we model the time-variant path delay as $\tau_\ell(t) = \tau_\ell(0) - f_\ell t/f_C$ for the duration of MT_S, where f_ℓ denotes the Doppler shift of path ℓ. With this assumption and using (4), we obtain

$$g'[n,q] = g_{\mathrm{Tx}}[q]_{\mathrm{Rx}}[q] \underbrace{\sum_{\ell=0}^{P-1} \eta_\ell \mathrm{e}^{-\mathrm{j}2\pi\theta_\ell\varphi(q)} e^{\mathrm{j}2\pi\nu_\ell n/(N+G)}}_{g_{\mathrm{Ph}}[n,q]} \tag{9}$$

where $\nu_\ell = f_\ell T_S$ denotes the normalized Doppler shift, and $\theta_\ell = \tau_\ell(0)/(NT_C)$ denotes the normalized path delay, respectively. The geometry-based wireless wave propagation model (9) is the basic foundation for the accurate emulation of vehicular wireless wave propagation properties. It was validated for modeling wireless communication channels for cellular [43]–[45] as well as vehicular communication systems [34].

As shown in previous investigations [34], [36], the channel response in vehicular environments consists of the sum of contributions coming from different reflecting objects, each one with strongly different statistical properties. The most important contributions stem from the following: the line-of-sight (LOS) path between transmitter and receiver; discrete objects, either mobile (MD) or static (SD), producing reflections with a larger time delay; diffuse scattering (D) coming from

reflections on side walls of the road. Therefore, we can rewrite $g_{\mathrm{Ph}}[n,q]$ as

$$\begin{aligned} g_{\mathrm{Ph}}[n,q] =& \eta_0^{(\mathrm{LOS})}[n] e^{-\mathrm{j}2\pi\theta_0^{(\mathrm{LOS})}\varphi(q)} e^{\mathrm{j}2\pi\nu_0^{(\mathrm{LOS})}n/(N+G)} \\ &+ \sum_{\ell=1}^{N_{\mathrm{SD}}} \eta_\ell^{(\mathrm{SD})}[n] e^{-\mathrm{j}2\pi\theta_\ell^{(\mathrm{SD})}\varphi(q)} e^{\mathrm{j}2\pi\nu_\ell^{(\mathrm{SD})}n/(N+G)} \\ &+ \sum_{\ell=1}^{N_{\mathrm{MD}}} \eta_\ell^{(\mathrm{MD})}[n] e^{-\mathrm{j}2\pi\theta_\ell^{(\mathrm{MD})}\varphi(q)} e^{\mathrm{j}2\pi\nu_\ell^{(\mathrm{MD})}n/(N+G)} \\ &+ \sum_{\ell=1}^{N_{\mathrm{D}}} \eta_\ell^{(\mathrm{D})}[n] e^{-\mathrm{j}2\pi\theta_\ell^{(\mathrm{D})}\varphi(q)} e^{\mathrm{j}2\pi\nu_\ell^{(\mathrm{D})}n/(N+G)} \end{aligned} \quad (10)$$

where N_{SD}, N_{MD}, and N_{D} denote the number of scattering objects (SD, MD, and D) (cf. [34, eq. (9)]). The detailed parameterization of (10) will be discussed in Section VII-B2.

IV. Generalized Discrete Prolate Speroidal Subspace Channel Model

We consider an OFDM system transmitting data frames over a time-variant frequency-selective channel. Pilot symbols are interleaved with data symbols in the time–frequency plane. Hence, we can observe the time-variant and frequency-selective channel for a certain region in time and frequency during the transmission of a single frame.

For channel estimation, we are interested to represent the channel in time and frequency by a low dimensional subspace such that a low-complexity reduced-rank (robust) Wiener filter [29] can be employed. For channel estimation, we are interested to design a subspace that minimizes the MSE. In general, this requires knowledge of the second-order statistics. The eigenvectors of the covariance matrix, i.e., the Karhunen–Loéve expansion [47], are the optimal basis functions spanning the subspace (see [17] for treatment in the frequency-domain approach and [32, Sec. III-C] for the time-domain approach, respectively). However, vehicular communication channels show local stationarity only, i.e., their second-order statistics can change rapidly. Hence, estimation of second-order statistics in frame-based communication systems is either difficult or impossible.

In Section IV-A, we introduce the concept of generalized DPS sequences, and we motivate and explain their application for a 2-D subspace model for time-variant frequency-selective channels in Section IV-B.

A. Generalized DPS Sequences

The subspace U spanned by time-limited snapshots of a band-limited (flat) fading process has an essential dimension given by the time–bandwidth product [32]

$$D'(\mathcal{W}, M) = \lceil |\mathcal{W}| M \rceil + 1 \quad (11)$$

where the interval

$$\mathcal{W} = \bigcup_{i=1}^{I} \mathcal{B}_i = \mathcal{B}_1 \cup \mathcal{B}_2 \cup \ldots \cup \mathcal{B}_I \quad (12)$$

defines the band limit [32, eq. (16)] potentially consisting of I disjoint intervals. Each interval is defined as $\mathcal{B}_i = (\nu_{i1}, \nu_{i2}), i \in \{1, \ldots, I\}$, with $\nu_{11} \leq \nu_{12} \leq \ldots \leq \nu_{I1} \leq \nu_{I2}$. The Lebesgue measure of $\mathcal{W}$ reads

$$|\mathcal{W}| = \sum_{i=1}^{I} (\nu_{i2} - \nu_{i1}). \quad (13)$$

The same subspace U is also spanned by generalized DPS sequences $\{u_i[m, \mathcal{W}, M]\}, i \in \{0, \ldots, M-1\}\}$, time limited to $m \in \mathcal{I}_M$. The generalized DPS sequences are band limited to the region $\mathcal{W}$, and their energy is most concentrated in the interval $\mathcal{I}_M$ (see [32, Def. 2]). They are the solutions to

$$\sum_{\ell=0}^{M-1} C[\ell - m, \mathcal{W}] u_i[\ell, \mathcal{W}, M] = \lambda_i(\mathcal{W}, M) u_i[m, \mathcal{W}, M] \quad (14)$$

for $m \in \mathbb{Z}$, where

$$C[k, \mathcal{W}] = \int_{\mathcal{W}} e^{\mathrm{j}2\pi k\nu} \mathrm{d}\nu \quad (15)$$

$$\lambda_i(\mathcal{W}, M) = \frac{\sum_{m=0}^{M-1} |u_i[m, \mathcal{W}, M]|^2}{\sum_{m=-\infty}^{\infty} |u_i[m, \mathcal{W}, M]|^2} \quad (16)$$

denotes the ith ordered eigenvalue also representing the energy concentration of $u_i[m, \mathcal{W}, M]$ within $\mathcal{I}_M$.

Note that $C[k, \mathcal{W}]$ is proportional to the covariance function of a process exhibiting a constant spectrum with support $\mathcal{W}$. Equation (15) evaluates to

$$C[k, \mathcal{W}] = \frac{1}{\mathrm{j}2\pi k} \sum_{i=1}^{I} \left(e^{\mathrm{j}2\pi k\nu_{i2}} - e^{\mathrm{j}2\pi k\nu_{i1}} \right) \quad (17)$$

if the band-limiting region $\mathcal{W}$ consists of I disjoint intervals.

B. Two-Dimensional Generalized DPS Channel Model

For a highly oversampled fading process $|\mathcal{W}| \ll 1$, the essential subspace dimension $D'(\mathcal{W}, M) \ll M$. This is the typical situation for modern high-rate communication systems. Due to the small degrees of freedom, the detailed shape of the power spectral density becomes less important for the estimation error. Hence, the support of the power spectral density is the crucial parameter for subspace design [13], [32] only. A similar reasoning was used for a robust Wiener filter design in [19] and [48].

Motivated by the structure of (9), we will represent $g[m,q]$ using a 2-D subspace model

$$\begin{aligned} g[m,q] \approx& \sum_{i=0}^{D_t-1} \sum_{k=0}^{D_f-1} u_i[m, \mathcal{W}_t, M] \\ &\cdot u_k \left[\varphi(q) + \frac{N}{2}, \mathcal{W}_f, N \right] \psi_{i,k} \end{aligned} \quad (18)$$

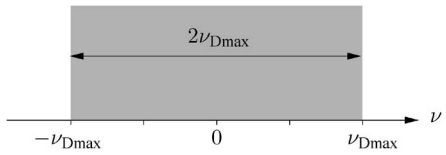

Fig. 2. Symmetric time-domain subspace $\mathcal{W}_t = [-\nu_{\mathrm{Dmax}}, \nu_{\mathrm{Dmax}}]$.

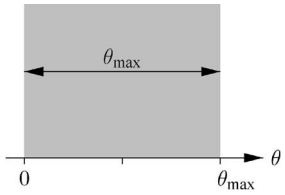

Fig. 3. Asymmetric frequency-domain subspace $\mathcal{W}_f = [0, \theta_{\max}]$.

where $\{u_i[m, \mathcal{W}_t, M], m \in \mathcal{I}_M, i \in \mathcal{I}_{D_t}\}$ spans the time-domain subspace, and $\{u_k[q, \mathcal{W}_f, N], q \in \mathcal{I}_N, k \in \mathcal{I}_{D_f}\}$ spans the frequency-domain subspace [30]. The generalized DPS coefficients are denoted by $\psi_{i,k}$.

The time-domain subspace $\{u_i[m, \mathcal{W}_t, M], m \in \mathcal{I}_M, i \in \mathcal{I}_{D_t}\}$ models a sequence in time, i.e., the channel coefficients $g[m, q]$ for a single subcarrier q and a finite time period $m \in \mathcal{I}_M$. The time-domain subspace is parameterized by the maximum support of the Doppler power spectral density $\mathcal{W}_t = [-\nu_{\mathrm{Dmax}}, \nu_{\mathrm{Dmax}}]$ (see Fig. 2).

Similarly, the frequency-domain subspace $\{u_k[q, \mathcal{W}_f, N], q \in \mathcal{I}_N, k \in \mathcal{I}_{D_f}\}$ models $g[m, q]$ for a single OFDM symbol m and a finite frequency interval $q \in \mathcal{I}_N$. The frequency-domain subspace is parameterized by the maximum support of the power delay profile $\mathcal{W}_f = [0, \theta_{\max}]$, where $\theta_{\max} = \tau_{\max}/(NT_C)$, and $\tau_{\max}$ is the maximum excess delay (see Fig. 3).

The subspace dimensions $D_t(\mathcal{W}_t, M)$ and $D_f(\mathcal{W}_f, N)$ minimizing the MSE for a given SNR can be expressed as [32], [49]

$$D(\mathcal{W}, M) = \underset{\mathcal{D} \in \{1,\ldots,M\}}{\arg\min} \left(\frac{1}{|\mathcal{W}|M} \sum_{i=\mathcal{D}}^{M-1} \lambda_i(\mathcal{W}, M) + \frac{\mathcal{D}}{M} \sigma_n^2 \right). \tag{19}$$

V. Iterative Channel Estimation

After inserting the subspace channel model (18) into the signal model (6), we obtain

$$y[m,q] = \left(\sum_{i=0}^{D_t-1} \sum_{k=0}^{D_f-1} u_i[m, \mathcal{W}_t, M] \cdot u_k \left[\varphi(q) + \frac{N}{2}, \mathcal{W}_f, N \right] \psi_{i,k} \right) d[m,q] + z[m,q]. \tag{20}$$

Using the generalized DPS sequences, our channel estimation problem is reduced to estimating the coefficients $\psi_{i,k}$. Note that $D_t D_f \ll NM$.

For the purpose of estimating the generalized DPS coefficients $\psi_{i,k}$, we rewrite (20) in matrix vector notation as follows. We collect the coefficient $\psi_{i,k}$ in the vector

$$\boldsymbol{\psi} = [\boldsymbol{\psi}_0^{\mathrm{T}}, \ldots, \boldsymbol{\psi}_{D_t-1}^{\mathrm{T}}]^{\mathrm{T}} \tag{21}$$

where

$$\boldsymbol{\psi}_i = [\psi_{i,0}, \ldots, \psi_{i,D_f-1}]^{\mathrm{T}}. \tag{22}$$

We collect the received data values $y[m, q]$ for all m and q in one vector

$$\mathbf{y} = [y[0,0], \ldots, y[0,N-1], y[1,0], \ldots, y[1,N-1] \ldots, y[M-1,0], \ldots, y[M-1,N-1]]^{\mathrm{T}}. \tag{23}$$

Similarly, we define vector $\boldsymbol{d}$ containing the data values $d[m, q]$ and the noise vector $\boldsymbol{z}$ containing the noise values $z[m, q]$.

We define the vector

$$\mathbf{f}[m, \mathcal{W}_t, M] = [u_0[m, \mathcal{W}_t, M], \ldots, u_{D_t-1}[m, \mathcal{W}_t, M]]^{\mathrm{T}} \tag{24}$$

containing the elements of the generalized DPS basis functions for a given time index m.

Finally, we define the $MN \times D_t D_f$ matrix

$$\boldsymbol{\mathcal{D}} = \mathbf{D} \begin{bmatrix} \mathbf{f}[0, \mathcal{W}_t, M]^{\mathrm{T}} \otimes \mathbf{f}\left[\varphi(0) + \frac{N}{2}, \mathcal{W}_f, N\right]^{\mathrm{T}} \\ \vdots \\ \mathbf{f}[M-1, \mathcal{W}_t, M]^{\mathrm{T}} \otimes \mathbf{f}\left[\varphi(0) + \frac{N}{2}, \mathcal{W}_f, N\right]^{\mathrm{T}} \\ \vdots \\ \vdots \\ \mathbf{f}[0, \mathcal{W}_t, M]^{\mathrm{T}} \otimes \mathbf{f}\left[\varphi(N-1) + \frac{N}{2}, \mathcal{W}_f, N\right]^{\mathrm{T}} \\ \vdots \\ \mathbf{f}[M-1, \mathcal{W}_t, M]^{\mathrm{T}} \otimes \mathbf{f}\left[\varphi(N-1) + \frac{N}{2}, \mathcal{W}_f, N\right]^{\mathrm{T}} \end{bmatrix} \tag{25}$$

where $\boldsymbol{D} = \mathrm{diag}(\boldsymbol{d})$, allowing us to write the signal model to estimate the generalized DPS coefficient vector $\boldsymbol{\psi}$ as

$$\mathbf{y} = \boldsymbol{\mathcal{D}}\boldsymbol{\psi} + \mathbf{z}. \tag{26}$$

We use the soft-symbol feedback from the BCJR decoder [40] to enhance the channel estimates iteratively. In the first iteration, only the pilots are used. We define $\tilde{\boldsymbol{\mathcal{D}}}$ similar to (25), where we substitute $d[m, q]$ collected in $\boldsymbol{d}$ with

$$\tilde{d}[m,q] = \tilde{b}[m,q] + p[m,q] \tag{27}$$

containing the soft symbol feedback $\tilde{b}[m, q]$.

The soft symbols $\tilde{b}[m, q]$ are defined according to

$$\tilde{b}[\mathcal{S}_s] = \mathop{\mathbb{E}}_{b}^{(\mathrm{APP})} \{b[\mathcal{S}_s]\} \tag{28}$$

$$= \frac{1}{\sqrt{2}} \left(\mathop{\mathbb{E}}_{c}^{(\mathrm{APP})} \{c[2s]\} + \mathrm{j} \mathop{\mathbb{E}}_{c}^{(\mathrm{APP})} \{c[2s+1]\} \right) \tag{29}$$

for $s \in \mathcal{I}_S$, where

$$\mathop{\mathbb{E}}_{c}^{(\mathrm{APP})} \{c[m']\} = 2\mathrm{Pr}^{(\mathrm{APP})} \{c[m'] = +1 | \hat{c}[m']\} - 1 \tag{30}$$

calculates the expectation over the alphabet of c, which is $\{-1,+1\}$. By $\Pr^{(\mathrm{APP})}$, we denote the *a posteriori* probability (APP) for the code symbol being $+1$ if $\hat{c}[m']$ is observed, where $\hat{c}[m']$ is obtained from the equalizer output $\hat{d}[m,q]$ after demapping and deinterleaving [24] (see also Fig. 5).

The linear MMSE estimator for the generalized DPS coefficients $\boldsymbol{\psi}$ can be expressed as

$$\hat{\boldsymbol{\psi}} = \left(\tilde{\boldsymbol{\mathcal{D}}}^{\mathrm{H}}\boldsymbol{\Delta}^{-1}\tilde{\boldsymbol{\mathcal{D}}} + \boldsymbol{\mathcal{C}}_{\boldsymbol{\psi}}^{-1}\right)^{-1}\tilde{\boldsymbol{\mathcal{D}}}^{\mathrm{H}}\boldsymbol{\Delta}^{-1}\mathbf{y} \tag{31}$$

following the derivation in [24, eq. (30)–(39)], where

$$\boldsymbol{\mathcal{C}}_{\boldsymbol{\psi}} = \frac{1}{|\mathcal{W}_t\|\mathcal{W}_f|}\mathrm{diag}\left(\boldsymbol{\lambda}(\mathcal{W}_t,M)\otimes\boldsymbol{\lambda}(\mathcal{W}_f,N)\right) \tag{32}$$

$$\boldsymbol{\lambda}(\mathcal{W}_t,M) = [\lambda_0(\mathcal{W}_t,M),\ldots,\lambda_{D_t}(\mathcal{W}_t,M)]^{\mathrm{T}} \tag{33}$$

and

$$\begin{aligned}[\boldsymbol{\Delta}]_{m+Mq,m+Mq} = \sigma_z^2 &+ \frac{1}{|\mathcal{W}_t\|\mathcal{W}_f|}\\ &\cdot\sum_{k=0}^{D_t-1}\sum_{i=0}^{D_f-1}\lambda_i(\mathcal{W}_t,M)\lambda_k(\mathcal{W}_f,N)\\ &\cdot|u_i[m,\mathcal{W}_t,M]u_k[\varphi(q)+N/2,\mathcal{W}_f,N]|^2\\ &\cdot\left(1-\left|\tilde{d}[m,q]\right|^2\right).\end{aligned} \tag{34}$$

VI. Pilot Pattern Design

In time-variant channels, the channel coefficients change between OFDM symbols within a frame, which needs to be tracked by the channel estimator. This is particularly true for vehicular settings, where high Doppler spreads of the channel are to be expected. In these cases, the pilot structure plays a significant role on how well these changes can be tracked by a channel estimator.

As discussed in [1], the pilot placement in the time–frequency grid in general needs to fulfill the sampling theorem. The maximum excess delay $\tau_{\max}$ determines how dense pilot symbols must be transmitted in the frequency domain. Hence, the maximum pilot spacing Δ_f (number of subcarriers) will satisfy

$$\Delta_f \leq \frac{N}{\tau_{\max}B}. \tag{35}$$

The Doppler spread determines how dense pilot symbols must be placed in time. The maximum spacing Δ_t (number of OFDM symbols) will satisfy

$$\Delta_t \leq \frac{B}{2f_D(N+G)}. \tag{36}$$

Optimal pilot placement is discussed in [50] and [51].

A. Standard IEEE 802.11p Pilot Pattern

The pilot pattern of the IEEE 802.11 OFDM frame [3], [52] is shown in Fig. 4. After the so-called "short preamble" (not shown) for coarse timing estimation, the "long preamble" consists of two OFDM symbols containing pilot symbols only. Additionally, four subcarriers contain pilots throughout the whole OFDM frame. This pilot structure is usually termed a "block-comb" structure. It is particularly suited for quasi-static channels, where the block pilots are used for an initial channel estimate, whereas the comb pilots will ensure tracking of the phase for carrier frequency offset compensation.

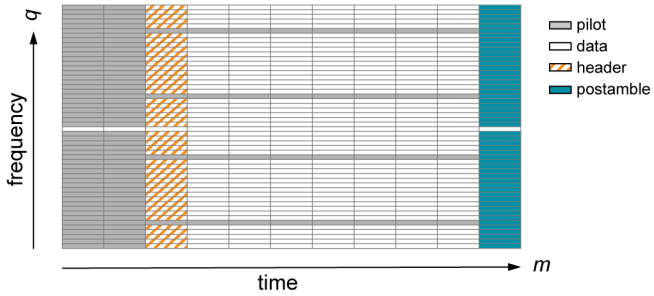

Fig. 4. Pilot pattern in an 802.11 OFDM frame extended by the proposed transparent postamble.

Using the bound (35), we can see that for a time-variant channel having an impulse response with $\tau_{\max} > 490$ ns, the 802.11p pilot pattern will cause degradation of the channel estimates due to aliasing.

For iterative receiver structures as discussed in this paper, the bounds (35) and (36) can be relaxed since the fed back soft symbols are used as additional pilot information. However, if (35) and (36) are strongly violated, the number of iterations until convergence increases or the iterative receiver convergence stops early [53]. In Section VII, we provide numeric simulation results further detailing the effect of the 802.11p pilot pattern on iterative channel estimation in vehicular channels.

B. Improved Pilot Pattern

The increased number of iterations needed due to the 802.11p pilot pattern that violates (35) and (36) leads to high computational complexity for hardware design. For this reason, we advocate to use an improved pilot symbol pattern by appending another OFDM pilot symbol as postamble to the OFDM frame, as indicated in Fig. 4. The existence of this postamble is announced in the "reserved" bit of the header structure [3].

It is known that this choice is still suboptimal for channel tracking [50], [51]. However, the advantage of this choice is that this pilot pattern is backwards compatible with the established standard, as follows.

1) New receivers check the value of the "reserved" bit in the header. When set, the postamble is used for improved channel estimation.
2) Conventional receivers ignore the "reserved" bit but obtain the number of OFDM symbols in a frame from the "length" field of the header. By that, they are simply ignoring the postamble.

With the postamble, the maximum excess delay is now determined by the cyclic prefix

$$\tau_{\max} < G/B \tag{37}$$

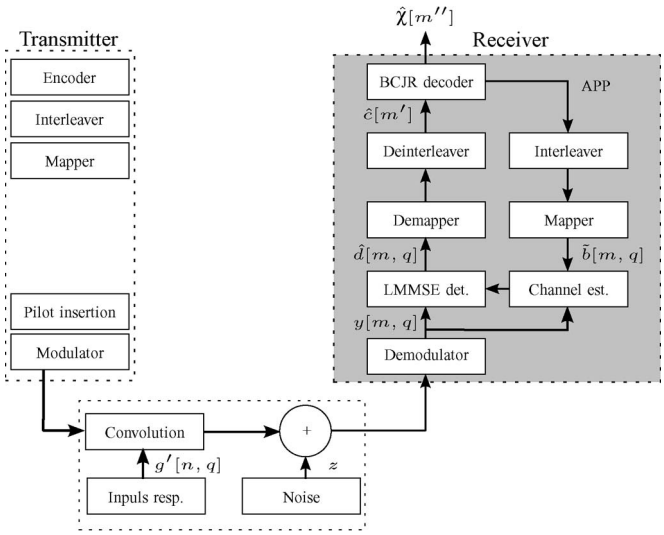

Fig. 5. Schematic structure of the 802.11p link-level simulator with iterative channel estimation.

and the maximum Doppler bandwidth depends on the frame length M

$$f_{\mathrm{Dmax}} < B/\left(2M(N+G)\right). \tag{38}$$

VII. Numeric Simulation Results

In this section, we present numerical simulation results obtained with an 802.11p-compliant link-level simulation.

A. IEEE 802.11p Link-Level Simulator

An 802.11p [3] compliant link-level simulator implemented in MATLAB is used to evaluate the iterative time-variant channel estimator. The building blocks of the simulator are depicted in Fig. 5, showing the transmitter, channel model, and receiver with iterative channel estimation.

The 802.11p standard uses a system bandwidth $B = 10$ MHz, and the cyclic prefix has length $G = 16$ samples, corresponding to a maximum tolerable excess delay of 1.6 μs (or 480 m propagation distance). Of the $N = 64$ subcarriers, only 52 are utilized for data transmission to provide upper and lower guard bands. We assume a carrier frequency of $f_C = 5.9$ GHz.

The 802.11p standard supports eight different coding and modulation schemes that allow for data rate adaptation ranging from 3 to 27 Mb/s [1, Sec. III-B]. In this paper, we present results using coding and modulation scheme 3 at 6 Mb/s. This scheme uses QPSK (with symbol mapper rate $R_{\mathrm{S}} = 2$) and a convolutional code with constraint length 7 and code rate $R_C = 1/2$.

We present simulation results for two different types of channel models for a vehicle driving at $v = 100$ km/h ≈ 28 m/s ≈ 62 mi/h communicating with a fixed infrastructure access point (vehicle-to-infrastructure):

1) A Rayleigh fading channel with an exponentially decaying power delay profile with root mean square (RMS) delay spread $\tau_{\mathrm{RMS}} = 0.4$ μs and a Clarke Doppler spectrum [54] for each tap modeling a non-LOS (NLOS) scenario (e.g., the LOS to the infrastructure access point is blocked by another vehicle). This model is similar to the "RTV-Expressway" tap delay line model described in [55].
2) A GSCM [34] implementing a vehicle-to-infrastructure scenario shown in [1, Fig. 18] that allows to model the nonstationary properties of the vehicle-to-infrastructure link with a dominant LOS propagation path (e.g., the access point is mounted on an elevated position on a motorway gantry).

Both channel models are implemented using fourfold oversampling. The bit error rate (BER) results will be shown versus E_b/N_0, where E_b denotes the energy per bit, and N_0 denotes the noise power spectral density. Hence, we calculate the variance of the additive symmetric complex white Gaussian noise according to

$$\frac{1}{\sigma_z^2} = \frac{E_b}{N_0} R_S R_C \frac{N}{N+G} \cdot \frac{M'}{M' + M_{\mathrm{Pr}} + M_{\mathrm{H}} + M_{\mathrm{Po}}} \frac{N_{\mathrm{Da}}}{N_{\mathrm{Da}} + N_{\mathrm{Pi}}} \tag{39}$$

where M', M_{Pr}, M_{H}, and M_{Po} are the numbers of OFDM symbols contained in the data, preamble, header, and postamble fields, respectively. The number of data subcarriers is denoted by N_{Da} and the number of pilot subcarriers by N_{Pi}. For all simulations, $N_{\mathrm{Da}} = 48$, $N_{\mathrm{Pi}} = 4$, $M_{\mathrm{Pr}} = 2$, $M_{\mathrm{H}} = 1$, and $M_{\mathrm{Po}} \in \{0, 1\}$, depending on the presence of the postamble pilot OFDM symbol. This corrects for the additional transmit energy used for the cyclic prefix, pilots, and header information. The generated channel impulse responses are normalized[1] to have average energy 1. Expressed by the time-variant frequency response, it reads

$$\mathbb{E}_m \left\{ \sum_{q=0}^{N-1} |g[m,q]|^2 \right\} = N \tag{40}$$

due to Parcevals's theorem. The transmitter sends a frame containing {200, 400, 800} bytes (B), which corresponds to a total frame length of $M = \{37, 71, 137\}$ OFDM symbols without postamble and $M = \{38, 72, 138\}$ with postamble, respectively. The presented results are averaged over 500 channel realizations for the NLOS scenario and over 1000 channel realization for the LOS scenario, respectively.

For the parameters of 802.11p and $M = 37$, (37) and (38) provide the following bounds: $\tau_{\max} < 1.6$ μs, and $f_D < 1.6$ kHz (300 km/h). These are sufficient for most vehicular scenarios.

B. Simulation Results

We will compare our simulations results with the baseline performance shown in [1] for the exponentially decaying power delay profile and Clarke's Doppler spectrum in NLOS

[1]For the GSCM (10), the normalization can be achieved since the attenuation of each path η_ℓ is known.

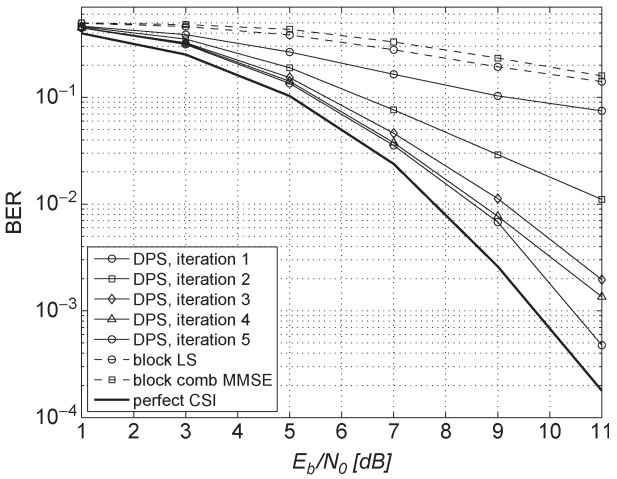

Fig. 6. BER versus E_b/N_0 for iteration $\{1, \ldots, 5\}$ for a frame length $M = 37$ and full 802.11p compliant (no postamble). The vehicles move at $v = 100$ km/h, and the channel model uses a Clarke Doppler profile for each channel tap. The power delay profile is exponentially decaying with RMS delay spread of 0.4 μs modeling a Rayleigh fading NLOS scenario.

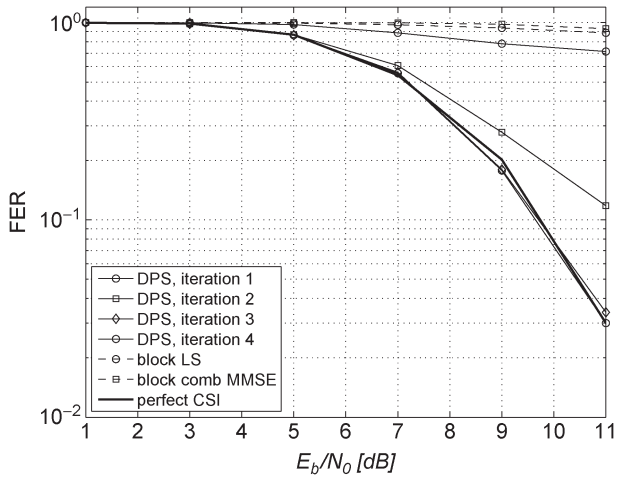

Fig. 7. FER versus E_b/N_0 for iteration $\{1, \ldots, 4\}$ for a frame length $M = 37$ and full 802.11p compliant (no postamble). The vehicles move at $v = 100$ km/h, and the channel model uses a Clarke Doppler profile for each channel tap. The power delay profile is exponentially decaying with RMS delay spread of 0.4 μs modeling a Rayleigh fading NLOS scenario.

situations as well as for the nonstationary model with strong LOS component.

In both cases, a noniterative least-square or linear MMSE estimator was used in [1] to demonstrate the current performance of common-of-the-shelf chip sets. A bit error floor at 10^{-1} for the NLOS case and at 10^{-4} for the LOS case at an $E_b/N_0 > 20$ dB was found in [1] due to the bad match of the 802.11p pilot pattern to a time-variant vehicular channel. A similar result is also reported in [56].

In the following, we will present numeric simulation results demonstrating the improved performance of the iterative receiver developed in this paper and the benefit of the modified backward compatible pilot pattern.

1) Vehicular NLOS Scenario: Fig. 6 shows the BER versus E_b/N_0 using the 802.11p compliant pilot pattern for channel estimation. The solid line without markers shows the BER with perfect channel state information (CSI) at the receiver side. The line with the circle markers shows the BER performance after the first iteration. Hence, a receiver without iterative channel estimation shows poor performance with a BER of about 10^{-1} at $E_b/N_0 = 11$ dB. Additionally, we show the baseline performance from [1] for the following: 1) the block least square estimator (block LS) where only the first two pilot symbols are used for channel estimation and 2) the block comb MMSE estimator where the four comb pilot subcarriers are employed to estimate the channel covariance function used then for MMSE channel estimation.

For a practical communication system, the FER is of high importance. In Fig. 7, we show the FER for the same scenario as in Fig. 6. Clearly, most frames can be received without error, and only a small number of frames contain multiple errors. Hence, the bit errors occur in bursts due to the time- and frequency-selective channel.

When the receiver makes reuse of the already decoded bits and their associated APPs, by running the receiver algorithm iteratively, the FER decreases and approaches the one for perfect CSI. We obtain FERs below 10^{-1} from the third iteration on, with the FER curve converging to that of perfect CSI after four iterations.

Nevertheless, the price we have to pay at the receiver side for this improvement is an increased complexity of the hardware implementation[2] (see Section VII-C for more details). To reduce this complexity, we evaluate our proposal to add an extra dedicated OFDM pilot symbol at the end of the frame, described previously as transparent postamble. This results in a strongly improved channel estimate already after the first iteration, as depicted in Fig. 8. An FER below 10^{-1} is obtained for $E_b/N_0 > 10.5$ dB with a distance of about 0.8 dB to the FER curve with perfect CSI. Convergence to the FER curve with perfect CSI is achieved already after the second iteration. Hence, the transparent postamble allows for a complexity reduction by a factor of 2 in the NLOS case analyzed in Figs. 7 and 8.

In Fig. 9, we plot the FER as a function of the number of iterations at the receiver for different frame sizes at a fixed $E_b/N_0 = 11$ dB. Circular markers depict results with the transparent postamble, the square markers are used for the ones without postamble, and the lines without markers show the FER obtained with perfect CSI. Different line styles are used to denote the length of the frame.

As expected, with increasing number of iterations, the FER converges toward the one with perfect CSI. The slope of the curves with transparent postamble is steeper than without postamble, indicating higher convergence speed. More precisely, the transparent postamble allows for a complexity reduction of at least a factor of 2 to reach an FER below 10^{-1} with a maximum number of two iterations for a frame size of 400 and 200 B. We reach an FER close to 10^{-1} after four iterations for 800 B frame size.

2) Vehicular LOS Scenario: The investigated scenario consists of a highway with two lanes in each direction, with a width

[2]For every iteration of the receiver, the chip area needs to be increased by an additional BCJR decoder, as well as frame storage, channel estimation, and data detection logic to allow for a continuous pipelined operation.

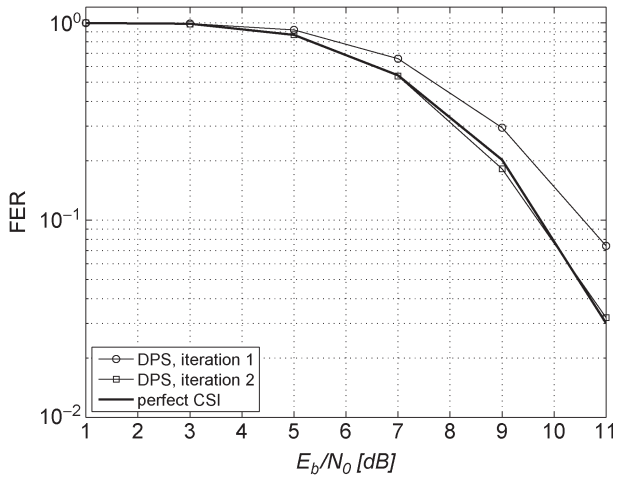

Fig. 8. FER versus E_b/N_0 for the first two iterations for a frame length of $M = 37$, with backward compatible transparent postamble. The vehicles move at $v = 100$ km/h, and the channel model uses a Clarke Doppler profile for each channel tap. The power delay profile is exponentially decaying with RMS delay spread of 0.4 μs.

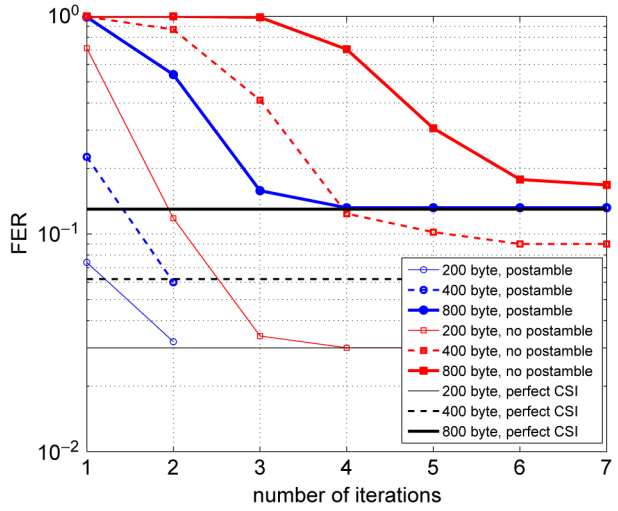

Fig. 9. FER versus number of iterations at an $E_b/N_0 = 11$ dB for varying frame size of {200, 400, 800} B. The vehicles move at $v = 100$ km/h, and the channel model uses a Clarke Doppler profile for each channel tap. The power delay profile is exponentially decaying with RMS delay spread of 0.4 μs.

of 4 m/lane. The transmitter is at a fixed position in the middle of the road at $x = 0$, which represents a road side unit, and the receiver in the onboard unit is moving on the outer lane with a velocity of 100 km/h (see [1, Fig. 18]).

We use a GSCM [34] with a parameterization for this specific vehicle-to-infrastructure scenario [57]. The parameterization in [34] was obtained from vehicle-to-vehicle measurements; however, since they describe the geometry of the surroundings, the parameters are only changed slightly for the vehicle-to-infrastructure scenario (see [57]). In Table I, we list the modifications of the parameterization relative to [34, Tab. I] for the different scattering objects in terms of the reference power G_0 and the pathloss exponent n.

The analysis of the BER is performed over 1000 generated channel realizations and at different x coordinates of the receiver $x \in \{50, 100, 200\}$ m. Other cars are also driving in both directions with a mean speed of 100 km/h $\approx$ 28 m/s and

TABLE I
GSCM PARAMETER MODIFICATIONS FOR THE VEHICLE-TO-INFRASTRUCTURE SCENARIO RELATIVE TO [34, TAB. I]. G_0 DENOTES THE REFERENCE POWER AND n THE PATHLOSS EXPONENT

Parameters	LOS	MD	SD	D
G_0 [dB]	-20	-80+24n	-80+24n	50
n	1.8	$\mathcal{U}$[0,3.5]	$\mathcal{U}$[0,3.5]	6.4

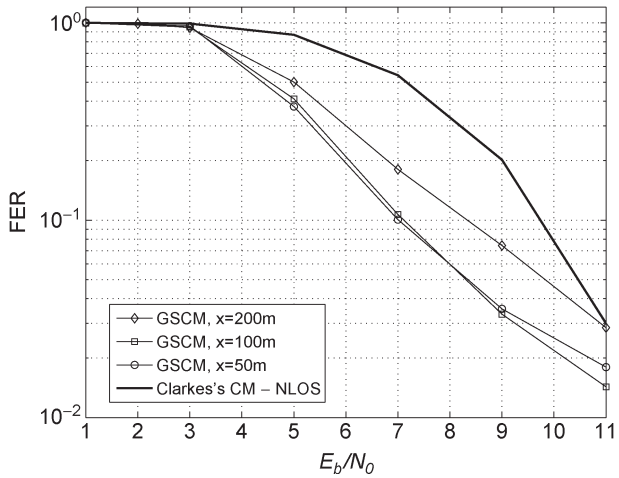

Fig. 10. FER with perfect CSI for different receiver coordinate $x = \{50, 100, 200\}$ m for the GSCM and NLOS. The frame length $M = 37$ contains 200 B.

standard deviation of 20 km/h $\approx$ 5.5 m/s. A band of objects producing diffuse scattering is placed beside the road (on both sides) with a width of 5 m.

For the investigation presented in this paper, we evaluate the FER versus E_b/N_0 for different positions x. Due to the strongly varying delay spread, Doppler spread, and Rician K-factor, the available diversity in the channel changes with x. To provide a baseline performance, we plot the FER with perfect CSI for all positions x in Fig. 10. The solid line in Fig. 10 depicts the FER for the NLOS Rayleigh fading scenario with exponentially decaying power delay profile and Clarke Doppler spectrum. Clearly, for the scenarios with strong LOS component, the diversity varies with x, and the NLOS channel provides highest diversity. However, for $E_b/N_0 < 11$ dB, the LOS scenario allows for smaller FERs.

Finally, in Fig. 11 we plot the FER versus the number of iterations for the LOS scenarios with receiver positions $x \in \{50, 100, 200\}$ m at a fixed $E_b/N_0 = 11$ dB. Again, we can demonstrate that the transparent postamble allows for a faster convergence of the iterative receiver with a complexity reduction of a factor of 2, reaching an FER smaller than 10^{-1} after one iteration.

For the presented simulation results, we use channel impulse responses normalized to unit average energy [see (40)]. However, in a practical receiver, the additive noise power stays constant and the signal energy will vary with x. The measured received energy over x is shown, e.g., in [46, Fig. 3], with a path loss exponent of $n = 1.8$. Hence, if we assume that we have $E_b/N_0 = 13$ dB when the receiver is at coordinate $x = 50$ m, the actual E_b/N_0 for the other distances is going to decrease, as indicated in Fig. 12. Therefore, the FER achieved is going to increase not only due to the fact that the channel properties

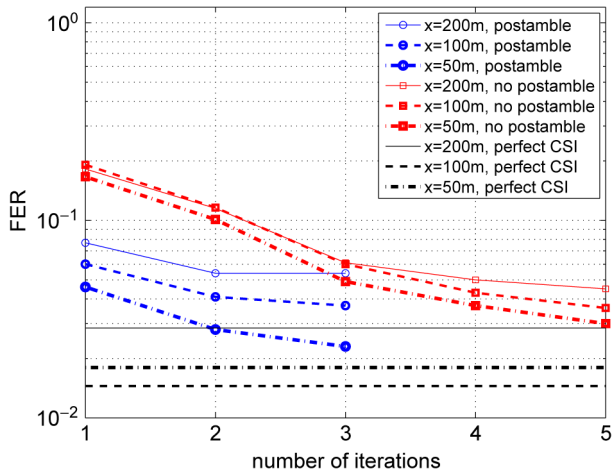

Fig. 11. FER versus number of iterations at $E_b/N_0 = 11$ dB for varying receiver coordinates $x = \{50, 100, 200\}$ m. The vehicles move at $v = 100$ km/h, and a GSCM [34] is used that allows to model the nonstationary properties of the vehicle-to-infrastructure link with a dominant LOS propagation path.

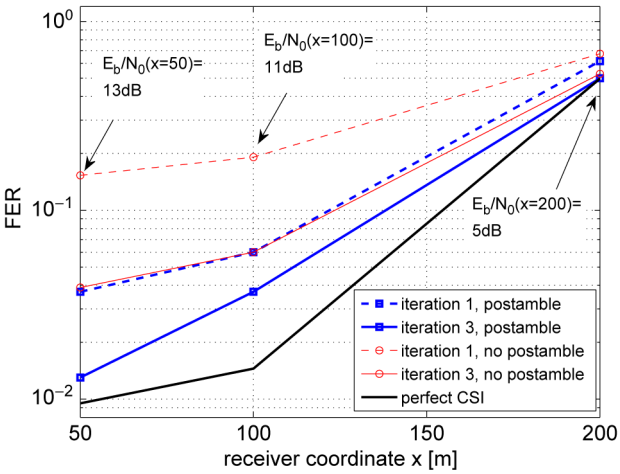

Fig. 12. FER versus receiver coordinate x for a given $E_b/N_0 = 13$ dB at distance $x = 50$ m.

vary with x but because E_b/N_0 is going to be different as well, depending on the distance. Noteworthy here again is that the FER obtained after the first iteration using the postamble is similar to the FER after three iterations without postamble.

C. Complexity

The new iterative algorithm presented in this paper together with the transparent postamble allows to operate 802.11p system in time-variant NLOS scenarios with an FER below 10^{-1}. Due to the legacy pilot pattern, a 2-D filter must be employed to achieve convergence.

The complexity of the iterative channel estimator is determined by three factors:

1) We employ a reduced rank 2-D linear MMSE filter (31), i.e., a reduced rank Wiener filter that allows to reduce the complexity compared with a normal Wiener filter [20] by utilizing only the dominant subspace. The complexity C_{RR} of the reduced rank filter (31) in terms of floating point operations [58] is determined by the dimension of matrix $\tilde{\boldsymbol{\mathcal{D}}} \in \mathbb{C}^{MN \times D_t D_f}$, as explained in [25, eq. (4)], resulting in

$$C_{\mathrm{RR}} \approx 8MN(D_t D_f)^2 + \frac{8}{3}(D_t D_f)^3. \tag{41}$$

The full linear MMSE filter would require $C_{\mathrm{LMMSE}} \approx 32/3(MN)^3$. For a 200 B frame at $E_b/N_0 = 16$ dB, the frame consists of $M = 38$ OFDM symbols and subspace dimensions $D_t = 2$ and $D_f = 19$. Hence, the complexity reduction relative to the 2-D Wiener filter is $C_{\mathrm{LMMSE}}/C_{\mathrm{RR}} = 1.5 \cdot 10^{11}/2.8 \cdot 10^7 = 5.4 \cdot 10^3$. A further complexity reduction of the reduced rank Wiener filter (31) is possible by utilizing the Krylov subspace method (see [25] for more details).
2) The dominant factor in the computational complexity of the iterative channel estimator is by far the BCJR decoder. An efficient max. logMAP implementation [59] in C consumes more than 85% of CPU time in the numerical simulations of the iterative receiver. However, a BCJR decoder is currently state of the art for turbo decoding in Universal Mobile Telecommunications Systems (UMTS) and Long-Term Evolution (LTE) receivers, and efficient max. logMAP VLSI implementations are readily available (see [59]).
3) As shown by the simulation results, two to three iterations are sufficient for most relevant scenarios. For the concrete chip set implementation, this means that the structure depicted in Fig. 5 in the gray box needs to be replicated I times, where I is the maximum number of iterations. This will allow a pipelined operation of the iterative algorithms.

VIII. Conclusion

We have presented an iterative reduced-rank channel estimator for vehicular time-variant channels based on generalized DPS sequences. This iterative algorithm allows convergence to the same BER and FER as with perfect CSI even when using the pilot pattern of the IEEE 802.11p standard. The 802.11p pilot pattern violates the sampling theorem for vehicular channels because it is identical to the one used in IEEE 802.11a, which was designed for indoor scenarios. To reduce the number of iterations and the complexity of the hardware implementation, we propose a backward-compatible pilot pattern modification by adding a postamble. This modified pilot pattern allows for a complexity reduction by a factor of 2–3. We present numerical simulation results using a tap delay line model and a GSCM, representing a Rayleigh fading NLOS situation and a strongly nonstationary LOS situation, respectively. For both scenarios, the robust performance was demonstrated to reach an FER below 10^{-1} after a maximum of three iterations with the added transparent postamble.

Acknowledgment

Parts of this work were performed as part of the project ROADSAFE, which is a scientific cooperation between FTW, ASFINAG, Kapsch TrafficCom, Fluidtime, and TU Wien, to improve vehicular communication systems.

REFERENCES

[1] C. F. Mecklenbräuker, A. F. Molisch, J. Karedal, F. Tufvesson, A. Paier, L. Bernadó, T. Zemen, O. Klemp, and N. Czink, "Vehicular channel characterization and its implications for wireless system design and performance," *Proc. IEEE*, vol. 99, no. 7, pp. 1189–1212, Jul. 2011.

[2] *IEEE Trial-Use Standard for Wireless Access in Vehicular Environments (WAVE)—Resource Manager*, IEEE Std. 1609.1-2006.

[3] *IEEE P802.11p: Part 11: Wireless LAN Medium Access Control (MAC) and Physical Layer (PHY) Specifications: Amendment 6: Wireless Access in Vehicular Environments*, IEEE Std. 802.11p-2010.

[4] A. F. Molisch, F. Tufvesson, J. Karedal, and C. F. Mecklenbräuker, "A survey on vehicle-to-vehicle propagation channels," *IEEE Wireless Commun.*, vol. 16, no. 6, pp. 12–22, Dec. 2009.

[5] A. Paier, R. Tresch, A. Alonso, D. Smely, P. Meckel, Y. Zhou, and N. Czink, "Average downstream performance of measured IEEE 802.11p infrastructure-to-vehicle links," in *Proc. IEEE ICC*, Cape Town, South Africa, May 23–27, 2010, pp. 1–5.

[6] L. Cheng, B. Henty, R. Cooper, D. Stancil, and F. Bai, "A measurement study of time-scaled 802.11 a waveforms over the mobile-to-mobile vehicular channel at 5.9 GHz," *IEEE Commun. Mag.*, vol. 46, no. 5, pp. 84–91, May 2008.

[7] J. Fernandez, D. Stancil, and F. Bai, "Dynamic channel equalization for IEEE 802.11p waveforms in the vehicle-to-vehicle channel," in *Proc. 48th Annu. Allerton Conf. Commun., Control, Comput.*, Sep. 29–Oct. 1, 2010, pp. 542–551.

[8] J. Fernandez, K. Borries, L. Cheng, V. Bhagavatula, D. Stancil, and F. Bai, "Performance of the 802.11p physical layer in vehicle-to-vehicle environments," *IEEE Trans. Veh. Technol.*, vol. 61, no. 1, pp. 3–14, Jan. 2012.

[9] A. Bourdoux, H. Cappelle, and A. Dejonghe, "Channel tracking for fast time-varying channels in IEEE802.11p systems," in *Proc. GLOBECOM*, Houston, TX, Dec. 2011, pp. 1–6.

[10] Y. Zhang, I. L. Tan, C. Chun, K. Laberteaux, and A. Bahai, "A differential OFDM approach to coherence time mitigation in DSRC," in *Proc. 5th ACM Int. Workshop Veh. Internetw.*, 2008, pp. 1–6.

[11] W. Cho, S. I. Kim, H. kyun Choi, H. S. Oh, and D. Y. Kwak, "Performance evaluation of V2V/V2I communications: The effect of midamble insertion," in *Proc. 1st Int. Conf. Wireless Commun., Veh. Technol., Inf. Theory Aerosp. Electron. Syst. Technol.*, May 2009, pp. 793–797.

[12] S. Sibecas, C. Corral, S. Emami, G. Stratis, and G. Rasor, "Pseudo-pilot OFDM scheme for 802.11a and R/A in DSRC applications," in *Proc. 58th IEEE VTC—Fall*, Oct. 2003, vol. 2, pp. 1234–1237.

[13] T. Zemen and C. F. Mecklenbräuker, "Time-variant channel estimation using discrete prolate spheroidal sequences," *IEEE Trans. Signal Process.*, vol. 53, no. 9, pp. 3597–3607, Sep. 2005.

[14] D. Slepian, "Prolate spheroidal wave functions, Fourier analysis, and uncertainty—V: The discrete case," *Bell Syst. Tech. J.*, vol. 57, no. 5, pp. 1371–1430, May/Jun. 1978.

[15] A. M. Sayeed, A. Sendonaris, and B. Aazhang, "Multiuser detection in fast-fading multipath environment," *IEEE J. Sel. Areas Commun.*, vol. 16, no. 9, pp. 1691–1701, Dec. 1998.

[16] D. Schafhuber, G. Matz, and F. Hlawatsch, "Adaptive Wiener filters for time-varying channel estimation in wireless OFDM systems," in *Proc. IEEE ICASSP*, Apr. 2003, vol. 4, pp. 688–691.

[17] O. Edfors, M. Sandell, J.-J. van de Beek, S. K. Wilson, and P. O. Börjesson, "OFDM channel estimation by singular value decomposition," *IEEE Trans. Commun.*, vol. 46, no. 7, pp. 931–939, Jul. 1998.

[18] J. Du and Y. G. Li, "D-BLAST OFDM with channel estimation," *EURASIP J. Appl. Signal Process.*, vol. 5, pp. 605–612, 2004.

[19] S. Kaiser, *Multi-Carrier CDMA Mobile Radio Systems—Analysis and Optimization of Detection, Decoding, and Channel Estimation*. Düsseldorf, Germany: VDI Verlag GmbH, 1998, ser. Fortschritts-Berichte VDI Reihe.

[20] S. Kaiser and P. Hoeher, "Performance of multi-carrier CDMA systems with channel estimation in two dimensions," in *Proc. 8th IEEE PIMRC*, Helsinki, Finland, Sep. 1997, vol. 1, pp. 115–119.

[21] A. Lampe and J. Huber, "Iterative interference cancellation for DS-CDMA systems with high system loads using reliability-dependent feedback," *IEEE Trans. Veh. Technol.*, vol. 51, no. 3, pp. 445–452, May 2002.

[22] G. Caire, R. R. Müller, and T. Tanaka, "Iterative multiuser joint decoding: Optimal power allocation and low-complexity implementation," *IEEE Trans. Inf. Theory*, vol. 50, no. 9, pp. 1950–1973, Sep. 2004.

[23] J. Wehinger and C. F. Mecklenbräuker, "Iterative CDMA multiuser receiver with soft decision-directed channel estimation," *IEEE Trans. Signal Process.*, vol. 54, no. 10, pp. 3922–3934, Oct. 2006.

[24] T. Zemen, C. F. Mecklenbräuker, J. Wehinger, and R. R. Müller, "Iterative joint time-variant channel estimation and multi-user detection for MC-CDMA," *IEEE Trans. Wireless Commun.*, vol. 5, no. 6, pp. 1469–1478, Jun. 2006.

[25] C. Dumard and T. Zemen, "Low-complexity MIMO multiuser receiver: A joint antenna detection scheme for time-varying channels," *IEEE Trans. Signal Process.*, vol. 56, no. 7, pp. 2931–2940, Jul. 2008.

[26] B. Hu, I. Land, L. Rasmussen, R. Piton, and B. Fleury, "A divergence minimization approach to joint multiuser decoding for coded CDMA," *IEEE J. Sel. Areas Commun.*, vol. 26, no. 3, pp. 432–445, Apr. 2008.

[27] S. Y. Park, Y. G. Kim, and C. G. Kang, "Iterative receiver for joint detection and channel estimation in OFDM systems under mobile radio channels," *IEEE Trans. Veh. Technol.*, vol. 53, no. 2, pp. 450–460, Mar. 2004.

[28] L. L. Scharf, *Statistical Signal Processing: Detection, Estimation, and Time Series Analysis*. Reading, MA: Addison-Wesley, 1991.

[29] F. A. Dietrich and W. Utschik, "Pilot-assisted channel estimation based on second-order statistics," *IEEE Trans. Signal Process.*, vol. 53, no. 3, pp. 1178–1193, Mar. 2005.

[30] T. Zemen, H. Hofstetter, and G. Steinböck, "Successive Slepian subspace projection in time and frequency for time-variant channel estimation," in *Proc. 14th IST IST SUMMIT*, Dresden, Germany, Jun. 2005.

[31] P. S. Rossi and R. R. Müller, "Slepian-based two-dimensional estimation of time-frequency variant MIMO-OFDM channels," *IEEE Signal Process. Lett.*, vol. 15, pp. 21–24, Jan. 2008.

[32] T. Zemen, C. F. Mecklenbräuker, B. H. Fleury, and F. Kaltenberger, "Minimum-energy band-limited predictor with dynamic subspace selection for time-variant flat-fading channels," *IEEE Trans. Signal Process.*, vol. 55, no. 9, pp. 4534–4548, Sep. 2007.

[33] L. Bernadó, N. Czink, T. Zemen, and P. Belanovic, "Physical layer simulation results for IEEE 802.11p using vehicular non-stationary channel model," in *Proc. IEEE ICC*, Cape Town, South Africa, May 2010, pp. 1–5.

[34] J. Karedal, F. Tufvesson, N. Czink, A. Paier, C. Dumard, T. Zemen, C. F. Mecklenbräuker, and A. F. Molisch, "A geometry-based stochastic MIMO model for vehicle-to-vehicle communications," *IEEE Trans. Wireless Commun.*, vol. 8, no. 7, pp. 3646–3657, Jul. 2009.

[35] S. B. Weinstein and P. M. Ebert, "Data transmission by frequency-division multiplexing using the discrete Fourier transform," *IEEE Trans. Commun.*, vol. COM-19, no. 5, pp. 628–634, Oct. 1971.

[36] Z. Wang and G. B. Giannakis, "Wireless multicarrier communications," *IEEE Signal Process. Mag.*, vol. 17, no. 3, pp. 29–48, May 2000.

[37] Y. G. Li and L. J. Cimini, "Bounds on the interchannel interference of OFDM in time-varying impairments," *IEEE Trans. Commun.*, vol. 49, no. 3, pp. 401–404, Mar. 2001.

[38] G. Faria, J. A. Henriksson, E. Stare, and P. Talmola, "DVB-H: Digital broadcast services to handheld devices," *Proc. IEEE*, vol. 94, no. 1, pp. 194–209, Jan. 2006.

[39] T. Luo, Z. Wen, J. Li, and H.-H. Chen, "Saturation throughput analysis of WAVE networks in Doppler spread scenarios," *IET Commun.*, vol. 4, no. 7, pp. 817–825, Apr. 2010.

[40] L. R. Bahl, J. Cocke, F. Jelinek, and J. Raviv, "Optimal decoding of linear codes for minimizing symbol error rate," *IEEE Trans. Inf. Theory*, vol. IT-20, no. 2, pp. 284–287, Mar. 1974.

[41] A. Paier, T. Zemen, L. Bernadó, G. Matz, J. Karedal, N. Czink, C. Dumard, F. Tufvesson, A. F. Molisch, and C. F. Mecklenbräuker, "Non-WSSUS vehicular channel characterization in highway and urban scenarios at 5.2 GHz using the local scattering function," in *Proc. WSA*, Darmstadt, Germany, Feb. 2008, pp. 9–15.

[42] O. Renaudin, V.-M. Kolmonen, P. Vainikainen, and C. Oestges, "Non-stationary narrowband MIMO inter-vehicle channel characterization in the 5-GHz band," *IEEE Trans. Veh. Technol.*, vol. 59, no. 4, pp. 2007–2015, May 2010.

[43] H. Hofstetter, "Characterization of the wireless MIMO channel," Ph.D. dissertation, Vienna Univ. Technol., Vienna, Austria, Sep. 2006.

[44] A. F. Molisch, "A generic channel model for MIMO wireless propagation channels in macro- and microcells," *IEEE Trans. Signal Process.*, vol. 52, no. 1, pp. 61–71, Jan. 2004.

[45] N. Czink, T. Zemen, J.-P. Nuutinen, J. Ylitalo, and E. Bonek, "A time-variant MIMO channel model directly parametrised from measurements," *EURASIP J. Wireless Commun. Netw.*, vol. 2009, p. 4, Feb. 2009.

[46] A. Paier, J. Karedal, N. Czink, C. Dumard, T. Zemen, F. Tufvesson, A. F. Molisch, and C. F. Mecklenbräuker, "Characterization of vehicle-to-vehicle radio channels from measurements at 5.2 GHz," *Wireless Pers. Commun.*, vol. 50, no. 1, pp. 19–32, Jul. 2009.

[47] A. Papoulis, *Probability, Random Variables and Stochastic Processes*. Singapore: McGraw-Hill, 1991.

[48] J. Berkmann, C. Carbonelli, F. Dietrich, C. Drewes, and W. Xu, "On 3G LTE terminal implementation—Standard, algorithms, complexities and challenges," in *Proc. IWCMC*, Aug. 2008, pp. 970–975.
[49] L. L. Scharf and D. W. Tufts, "Rank reduction for modeling stationary signals," *IEEE Trans. Acoust., Speech, Signal Process.*, vol. ASSP-35, no. 3, pp. 350–355, Mar. 1987.
[50] L. Tong, B. Sadler, and M. Dong, "Pilot-assisted wireless transmissions: General model, design criteria, and signal processing," *IEEE Signal Process. Mag.*, vol. 21, no. 6, pp. 12–25, Nov. 2004.
[51] R. Mersereau, "The processing of hexagonally sampled two-dimensional signals," *Proc. IEEE*, vol. 67, no. 6, pp. 930–949, Jun. 1979.
[52] *Supplement to IEEE Standard for Information Technology-Telecommunications and Information Exchange Between Systems—Local and Metropolitan Area Networks—Specific Requirements. Part 11: Wireless LAN Medium Access Control (MAC) and Physical Layer (PHY) Specifications: High-Speed Physical Layer in the 5 GHz Band*, IEEE Std. 802.11a-1999.
[53] S. ten Brink, "Convergence of iterative decoding," *Electron. Lett.*, vol. 35, no. 10, pp. 806–808, May 1999.
[54] R. H. Clarke, "A statistical theory of mobile-radio reception," *Bell Syst. Tech. J.*, vol. 47, pp. 957–1000, Jul./Aug. 1968.
[55] G. Acosta-Marum and M. A. Ingram, "Six time- and frequency-selective empirical channel models for vehicular wireless LANs," *IEEE Veh. Technol. Mag.*, vol. 2, no. 4, pp. 4–11, Dec. 2007.
[56] I. Ivan, P. Besnier, M. Crussiere, M. Drissi, L. Le Danvic, M. Huard, and E. Lardjane, "Physical layer performance analysis of V2V communications in high velocity context," in *Proc. 9th ITST*, Oct. 2009, pp. 409–414.
[57] A. Paier, J. Karedal, N. Czink, H. Hofstetter, C. Dumard, T. Zemen, F. Tufvesson, and A. Molisch, "First results from car-to-car and car-to-infrastructure radio channel measurements at 5.2 GHz," in *Proc. 18th IEEE PIMRC*, Athens, Greece, Sep. 2007, pp. 224–228.
[58] G. H. Golub and C. F. V. Loan, *Matrix Computations*, 3rd ed. Baltimore, MD: The Johns Hopkins Univ. Press, 1996.
[59] L. Sabeti, M. Ahmadi, and K. Tepe, "Low-complexity BCJR decoder for turbo decoders and its VLSI implementation in 0.18-μm CMOS," in *Proc. 62nd IEEE VTC—Fall*, Sep. 2005, vol. 2, pp. 912–916.

Thomas Zemen (S'03–M'05–SM'10) received the Dipl.-Ing. degree (with distinction) in electrical engineering from the Vienna University of Technology, Vienna, Austria, in 1998 and the doctoral degree (with distinction) in 2004.

From 1998 to 2003, he was a Hardware Engineer and Project Manager with the Radio Communication Devices Department, Siemens Austria. Since October 2003, he has been with FTW Forschungszentrum Telekommunikation Wien, Vienna, where he has been leading the Department of "Signal and Information Processing" since 2008. He is the speaker of the national research network for "Signal and Information Processing in Science and Engineering" funded by the Austrian Science Fund (FWF). His research interests include vehicular channel measurements and modeling, time-variant channel estimation, orthogonal frequency-division multiplexing, iterative multiple-input–multiple-output receiver structures, cooperative communication systems, and interference management. He teaches as External Lecturer with the Vienna University of Technology and serves as Editor for the IEEE TRANSACTIONS ON WIRELESS COMMUNICATIONS. He is the author or coauthor of four book chapters and more than 80 journal papers and conference communications.

Laura Bernadó (S'09) received the M.Sc. degree from the Technical University of Catalonia, Barcelona, Spain. She is currently working toward the doctoral degree with the Vienna University of Technology, Vienna, Austria.

She is currently a Researcher in safety-related vehicular communications projects with the Telecommunications Research Center Vienna (FTW), Vienna. Her Master's thesis was written while with the Radio Communications Department, Royal Institute of Technology, Stockholm, Sweden. Her research interests are the modeling of fast time-varying fading processes and, particularly, characterization of nonstationarity for vehicular channels.

Nicolai Czink (S'04–M'08) received the Dipl.-Ing. (M.S.) degree in 2004 and the Dr.techn. (Ph.D.) degree in 2007 (with distinction) from the Vienna University of Technology, Vienna, Austria.

After his Ph.D., he joined Stanford University, Stanford, CA, as a Postdoctoral Researcher on an Erwin Schrödinger Fellowship of the FWF Austrian Science Fund. After that, he became a Senior Researcher with the FTW Telecommunications Research Center Vienna, where he works on channel modeling, cooperative communications, and intelligent transportation systems.

Dr. Czink's thesis received an award from the Austrian Electrotechnical Association.

Andreas F. Molisch (S'89–M'95–SM'00–F'05) received the Dipl. Ing., Ph.D., and habilitation degrees from the Technical University of Vienna, Vienna, Austria, in 1990, 1994, and 1999, respectively.

He subsequently was with AT&T (Bell) Laboratories Research (USA); Lund University, Lund, Sweden, and Mitsubishi Electric Research Labs (USA). He is now a Professor of electrical engineering with the University of Southern California, Los Angeles. His current research interests are the measurement and modeling of mobile radio channels, ultra-wideband communications and localization, cooperative communications, multiple-input–multiple-output systems, and wireless systems for healthcare. He has authored, coauthored, or edited four books (among them the textbook *Wireless Communications*, Wiley-IEEE Press), 14 book chapters, more than 130 journal papers, and numerous conference contributions, as well as more than 70 patents and 60 standards contributions.

Dr. Molisch has been an Editor of a number of journals and special issues, General Chair, Tecnical Program Committee Chair, or Symposium Chair of multiple international conferences, as well as Chairman of various international standardization groups. He is a Fellow of the IET, an IEEE Distinguished Lecturer, and a member of the Austrian Academy of Sciences. He has received numerous awards, most recently the 2011 James Evans Avant-Garde award of the IEEE Vehicular Technology Society and the Donald Fink Prize of the IEEE.